Quantitative characterization of pore-scale disorder effects on transport in "homogeneous" granular media

Andrea Cortis,* Youjian Chen,† Harvey Scher,‡ and Brian Berkowitz§
Department of Environmental Sciences and Energy Research, Weizmann Institute of Science, 76100 Rehovot, Israel
(Received 14 May 2004; published 28 October 2004)

Breakthrough curves (BTC) of a passive tracer in macroscopically homogeneous granular materials (well-sorted, unconsolidated sands or glass beads) were measured in a series of column experiments. The early and late arrival times are observed to differ systematically from theoretical predictions based on solution of the advective-dispersion equation for uniform porous media. We propose that subtle and residual pore-scale disorder effects in the porous media can account for these observations. We determine an ensemble-averaged distribution of particle transfer rates (based on a master equation for the local flux-averaged concentration) which incorporates these effects, and utilize it to calculate BTC that are in excellent agreement with the entire series of observations. Theoretical prediction of the dependence of the effective macroscopic parameters on measurable quantities is also in excellent agreement with the observations.

DOI: 10.1103/PhysRevE.70.041108 PACS number(s): 05.40.Fb, 05.60.-k, 02.50.-r, 45.70.-n

I. INTRODUCTION

Since the seminal study of Taylor [1], the transport of a passive tracer in macroscopically homogeneous granular materials, under an advecting steady flow, has been treated by analogy to the classical (Fickian) diffusion problem in a homogeneous fluid. As a consequence, the advection-dispersion equation (ADE),

$$n\frac{\partial}{\partial t}c(y,t) = -\nabla\cdot[qc(y,t) - D\nabla c(y,t)], \tag{1}$$

has long been regarded as the correct model to describe this kind of transport. In (1), c is the resident fluid concentration, n is porosity, $q=n\langle v\rangle$ is volumetric fluid flux per unit area, $\langle v\rangle$ the average fluid velocity, t is time, y is distance, and D is the hydrodynamic dispersion coefficient.

While the ADE has been documented to provide "average," large-scale descriptions of tracer migration in porous media, non-Fickian (or "anomalous") transport patterns are observed frequently. Such patterns are usually distinguished by early arrival and late time tails in breakthrough curves which differ from those described by the ADE. Anomalous dispersion of a passive tracer in porous media has often been associated with the presence of large scale heterogeneities. However, Scheidegger [2] already noted, nearly 45 years ago, that as compared to calculations from the classical ADE model, systematic deviations were observed in the early arrival times and long-time tails of breakthrough curves (BTC) measured in "homogeneous" sandstones.

The question of the scale or conditions under which a porous medium can be considered "homogeneous" therefore arises naturally. For example, the existence of preferential flow paths and non-Fickian tracer transport even in small scale, "homogeneously" packed column experiments was shown clearly by, e.g., Hoffman *et al.* [3] and Oswald *et al.* [4]. Similar behavior was demonstrated in meter scale flow cells by Silliman and Simpson [5] and Levy and Berkowitz [6]. A recent reanalysis [7] of the data reported in [2], as well as from other experiments on tracer transport in small scale, natural ("homogeneous") soil columns [8,9], further examined and quantified the occurrence of non-Fickian transport.

We argue that in "uniform" porous media, the ADE framework may provide a good description of the mean arrival time (which correlates to the mean Stokes flow $\langle v\rangle$), but cannot account for a precise description of tracer transport (e.g., early and late tracer arrival times) due to fluctuations in mean behavior. The key issue is to recognize that short-range "geometrical" heterogeneity in a porous medium leads also to short-range spatial variability in the microscopic velocity field $v(y)$ of the liquid that carries the tracer. These latter effects are eventually "averaged out" in, e.g., sufficiently long columns L of granular matter: $L >>> d_m$, where d_m is a characteristic diameter of the individual grains. However, in a large range, where $L \gg d_m$, these fluctuations can produce the measurably systematic deviations from the BTC described by the ADE.

In the present work, we have measured the transport of a passive tracer in macroscopically "homogeneous" granular materials, for a range of steady advective flow rates and for a series of different well-sorted, unconsolidated sands and glass beads. We demonstrate that even microscopic changes in the velocity distribution—in this case, given by relative changes in the random fluctuations around a mean liquid velocity in a macroscopically homogeneous porous medium—can lead to distinct, quantifiable patterns in the early arrival times and long-time tailing behavior. We also show that this behavior cannot be quantified by the classical ADE model. It is important to note here that we use exact solutions for the ADE (and our proposed model) that account explicitly for the length of the column and the appropriate inlet and outlet boundary conditions. Therefore, our fits with

*Electronic address: andrea.cortis@weizmann.ac.il
†Electronic address: youjian.chen@weizmann.ac.il
‡Electronic address: harvey.scher@weizmann.ac.il
§Electronic address: brian.berkowitz@weizmann.ac.il

the ADE are not affected by fitting artifacts of the classical analytical ADE solution for an infinite length column.

We approach our theoretical analysis of the subtle effects of pore-scale disorder within a framework that has been highly successful in accounting for anomalous transport in strongly heterogeneous media—the continuous time random walk (CTRW) formalism [10–12]. In this context, we have developed [13] generalized transport equations with the CTRW theory, and shown the ADE to be a highly constrained subset of this theory. The CTRW is characterized by $\psi(s,t)$, the probability rate of a local displacement s at transition time t. In many instances, it is possible to assume that the transition rate probability can be applied in the uncoupled form $\psi(s,t)=p(s)\psi(t)$, where $p(s)$ is the probability distribution of the length of the jumps and $\psi(t)$ is the probability rate for a transition time t between sites.

In this contribution, we consider the determination of $\psi(t)$ for the mildly disordered porous media used in our experiments. We develop a physical model based on a master equation (ME) for the flux concentration, containing the explicit pore-scale transitions. In Sec. II we present our experimental results and the comparison to the ADE predictions. In Sec. III we derive the $\psi(s,t)$ we use in the generalized transport equation computations of BTC, and in Sec. IV we compare these results to the experimental ones.

II. TRANSPORT EXPERIMENTS IN HOMOGENEOUS GRANULAR MATERIALS

We performed a series of tracer breakthrough experiments in a one-dimensional (1D) flow field, on uniformly packed columns of two different lengths. The filling material was well-rounded quartz sand with minimal surface coatings (UNIMIN Corporation, USA). Three grain sizes were used, namely fine, medium, and coarse sand, with average grain diameters of 0.231, 0.532, and 1.105 mm, respectively. Glass beads with an average diameter of 4.0 mm were also used.

The experiments used two "short" columns (one of length 19.70 cm and 2.478-cm internal diameter, and the other of length 19.85 cm and 2.512-cm internal diameter), and two "long" columns (with lengths 101.0 and 101.2 cm, and internal diameter of 2.785 cm). The inlet and outlet ends of each column were separated from the porous medium by thin nylon meshes with hydraulic conductivity larger than those of the sand and glass beads. Small open volumes between the meshes and the column closure caps served to promote tracer mixing and to further dampen subtle pulses in the injected liquid caused by the peristaltic pump.

Each sand packing was carried out under saturated conditions, with (sequentially) small amounts of sand being poured through water and stirred with a thin stick to avoid air entrapment. In addition, the sand was compacted and the column was shaken frequently during the process of packing. The porosity was controlled by weighing the amount of sand packed into a given column volume, allowing for different densities of the sands. This methodology ensured that the columns were as uniformly saturated and as homogeneous as possible.

The flow rate of the injected water and tracer (sodium chloride) was controlled by a peristaltic pump (Master FLEX, USA) together with a flow dampener. A T joint connected salt water and fresh water reservoirs, which enabled an immediate switch over between the different water supplies without interrupting the flow. In each experiment, fresh water was used to initiate and stabilize the flow, and to calibrate the background concentration. Salt water was then injected to displace the fresh water and to determine breakthrough curves. The effluent conductivity was measured over time with an electrical conductivity (EC) meter (TWIN, Japan), with maximum measurement error of 1%, and then converted to tracer concentration values by using calibration curves. All tracer experiments were run until the effluent conductivity was steady and equal to the inflow concentration, at a constant room temperature of 23 °C. In all experiments, fresh water was prepared from boiled, deionized water; salt water contained 500 mg/L NaCl.

To maximize the resolution and accuracy of the measurements, "dead volumes" of fluid (containing both tube volume and inlet volume of column) were accounted for in the treatment of the measurements. For this purpose, a neutral-colored dye was injected to estimate the dead volume between source water switchover and column inlet: the time of flow through this switchover was deducted from the measured breakthrough times at the column outlet. The outlet volume of the columns was also minimized to increase the accuracy of the conductivity measurements of the effluent. The colored dye was also used to ensure that fluctuations in the flow rate could be considered negligible with regard to the outlet concentration measurements.

Figure 1 shows a typical BTC (normalized flux-averaged concentration j versus time t) for a short column filled with fine sand. It can be observed that while the mean arrival time is approximatively matched by the fitted ADE model, the predicted early and late arrival times deviate from the data. These deviations are found to be systematic and of comparable order of magnitude for the entire set of (48) short column experiments. Also shown in Fig. 1 is a fit to the data using a CTRW formulation to be derived and discussed below. Similarly, Fig. 2 shows a typical BTC for a long column filled with coarse sand. Here, it is evident that for this particular column length and packing, the ADE model correctly predicts the Fickian evolution of the experiment.

From this analysis, we conclude that there is a transition between the anomalous behavior observed in the short column experiments and the Fickian behavior characteristic of the long column. These considerations on length scales must of course be taken in relative terms. The ratio of the total length of the column to the diameter of the characteristic disorder (the diameter of the grains) is equal to $L/d_m=870$ for the short column (fine sand) experiment, and it is of the same order of magnitude for the long column (coarse sand) experiment, $L/d_m=909$. The degree of the heterogeneity is therefore comparable for the two cases. However, as the volumetric fluid fluxes are also comparable ($Q=6.717\times10^{-7}$ and 7.8760×10^{-7} m^3/min for the short and long columns, respectively), the residence time of the tracer in the long column ($\hat{t}\sim265$ min) is more than five times larger than that for the short column ($\hat{t}\sim53.7$ min). The relative resi-

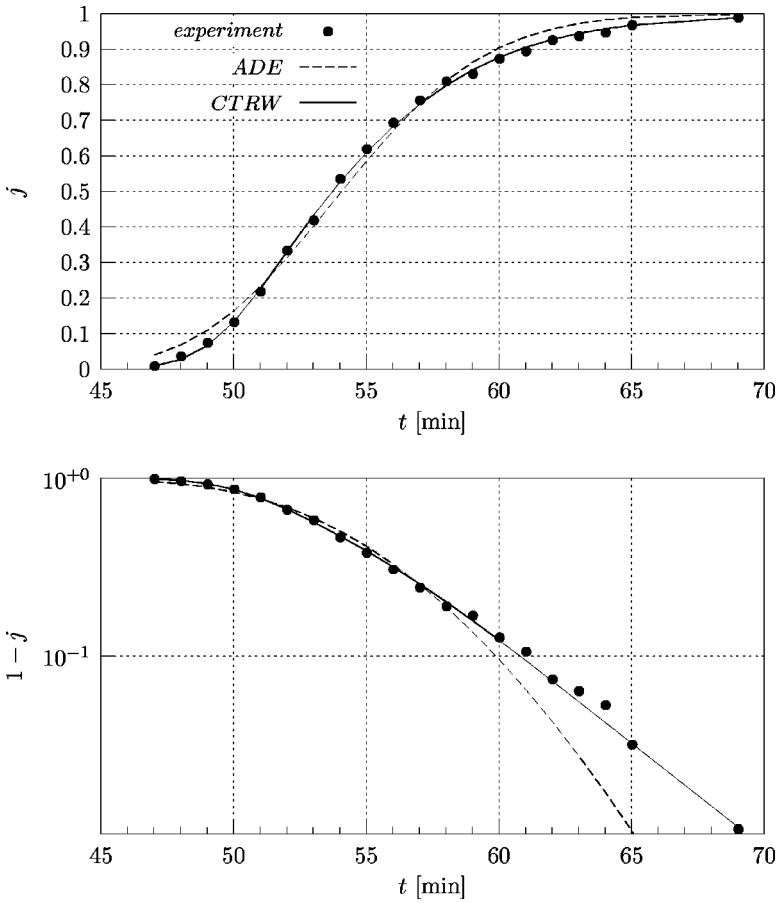

FIG. 1. Comparison of measured vs fitted breakthrough curves for a typical short column experiment. The quantity j represents the normalized flux-averaged concentration. Dots: measured chloride breakthrough curve, for a fine sand: $d_m = 0.231$ mm. Measured porosity $n = 0.3228$. Column length $L = 19.85$ cm. Section area $= 4.956 \times 10^{-4}$ m^2. Volumetric fluid flow $Q = 6.717 \times 10^{-7}$ m^3/min. Dashed line: best ADE model fit: $\langle v \rangle = 4.917 \times 10^{-3}$ m/min, $D = 3.2363 \times 10^{-6}$ m^2/min. Solid line: best CTRW fit: $v_\psi = 4.0389 \times 10^{-3}$ m/min, $D_\psi = 1.1601 \times 10^{-6}$ m^2/min, $\eta = 0.9212$. The lower figure shows the quantity $(1-j)$ in logarithmic units to emphasize the long-time tail.

dence time is ultimately what governs the transition from anomalous to a Fickian behavior. A rigorous, quantitative treatment of this anomalous behavior and the evolution towards Fickian behavior is described in the next section.

III. THE PHYSICS OF THE PROBLEM

A. Derivation of the $\psi(t)$

The complex nature of the paths traveled by the tracer is governed by the fluctuations of the Stokes velocity field $v(y)$ around its average value $\langle v(y) \rangle$ due to the local heterogeneities in the pore volume. It is expedient to consider local averages of the key quantities and retain a statistical characterization of these fluctuations. We consider a master equation for the flux-averaged concentration $\theta(y,t) = v(y)\Theta(y,t)$, where $\Theta(y,t)$ is the normalized resident concentration,

$$\frac{\partial \theta(y,t)}{\partial t} = -\sum_{y'} w(y',y)\,\theta(y,t) + \sum_{y'} w(y,y')\,\theta(y',t), \quad (2)$$

where $w(y,y')$ is the transition rate of tracer "particles" from y' to y in a single realization (units of t^{-1}) and the sum over y is, in principle, over the pores of the fluid volume. The

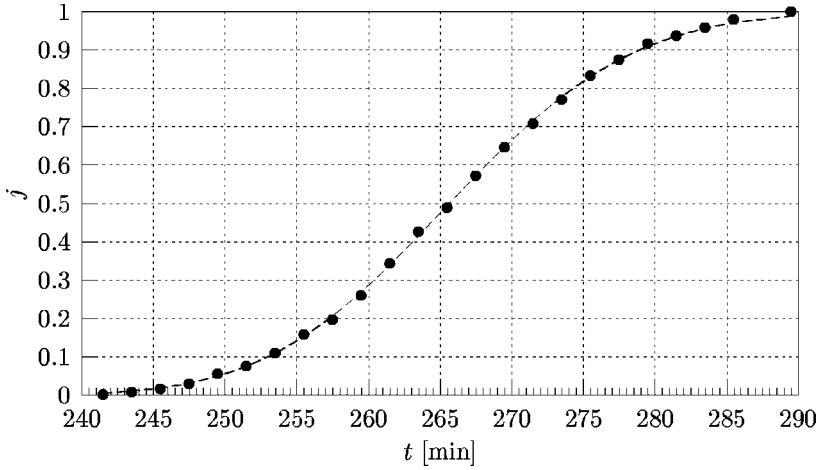

FIG. 2. Comparison of measured vs fitted breakthrough curves for a typical long column experiment. The quantity j represents the normalized flux-averaged concentration. Dots: measured chloride breakthrough curve, for a coarse sand: $d_m = 1.105$ mm. Measured porosity $n = 0.3262$. Column length $L = 101.2$ cm. Section area $= 6.0917 \times 10^{-4}$ m^2. Volumetric fluid flow $Q = 7.8760 \times 10^{-7}$ m^3/min. Dashed line: best ADE model fit: $\langle v \rangle = 3.8072 \times 10^{-3}$ m/min, $D = 2.7793 \times 10^{-6}$ m^2/min.

procedure to account for the statistics of the local fluctuations requires the use of a local average over some volume $V_{cell} \equiv (4/3)\pi r^3$, where $\langle f(y)\rangle \equiv 1/V_{cell}\int_{V_{cell}} f(y+\varsigma)d\varsigma$. Clearly, r is proportional to the characteristic length of the spatial particle transitions, $\ell = \Sigma_s p(s)s$. This *coarse-graining* procedure amounts to shifting the length scale from the interpore distance to the V_{cell} radius, r, and to designating an effective site density (see below). The probability rate $\psi(t)$ is related to the derivative of the ensemble-averaged part of the outgoing contribution in the ME for the concentration [see, e.g., [14]].

The physical model is determined by the expression for the transition rate $w(y',y)$ which we write as $w(y+s)$, where s is the distance to the appropriately averaged sites (i.e., contained in V_{cell}) of the configuration. The particles are transported by the flow, hence it is reasonable to assume

$$w(y+s) = \frac{a}{8}\frac{v(y+s)}{\ell} + \frac{b}{6\bar{t}}\exp\left(-\frac{s}{\lambda}\right), \tag{3}$$

with λ a characteristic diffusion length, and $\bar{t}$ a characteristic "relaxation time for diffusion." Note that the diffusion contribution decays exponentially with the distance from the considered point (Fickian diffusion). We incorporate all the remaining uncertainty in the expression for w in the two numerical constants a and b, which are determined experimentally. The factor $1/6$ is introduced for convenience to simplify the forthcoming algebra. Further discussion on the connection between $w(y+s)$ and $v(y+s)$, and on the origin of the $1/8$ coefficient, is given in the Appendix.

Averaging the outgoing contribution of the ME in (2), we can now write

$$-\frac{d}{dt}\langle\Theta(y,t)v(y)\rangle = \sum_s \langle\Theta(y,t)v(y)w(y+s)\rangle, \tag{4}$$

where we further assume that

$$\langle\Theta(y,t)v(y)\rangle = \langle\Theta(y,t)\rangle\langle v(y)\rangle \tag{5}$$

and

$$\left\langle\Theta(y,t)\left[\frac{a}{8\ell}v(y)v(y+s) + v(y)\frac{b}{6\bar{t}}\exp\left(-\frac{s}{\lambda}\right)\right]\right\rangle = \langle\Theta(y,t)\rangle\left[\frac{a}{8\ell}\langle v(y)v(y+s)\rangle + \langle v(y)\rangle\frac{b}{6\bar{t}}\exp\left(-\frac{s}{\lambda}\right)\right]. \tag{6}$$

We can then write (4) as

$$-\frac{d}{dt}\langle\Theta(y,t)\rangle = \frac{\langle\Theta(y,t)\rangle}{\langle v(y)\rangle}\sum_s\left[\frac{a}{8\ell}\langle v(y)v(y+s)\rangle + \langle v(y)\rangle\frac{b}{6\bar{t}}\exp\left(-\frac{s}{\lambda}\right)\right]. \tag{7}$$

The averaging volume V_{cell} is chosen to also contain the fluctuations of the local Stokes velocity field, which is specified by δ the correlation length (where $\delta < r$),

$$\langle v(y)v(y+s)\rangle = \langle v(y)^2\rangle\exp\left(-\frac{s}{\delta}\right). \tag{8}$$

We assume that the diffusion length $\lambda \sim \delta$. Substituting (8) into (7) we have

$$-\frac{d}{dt}\langle\Theta(y,t)\rangle = \langle\Theta(y,t)\rangle\left(\frac{a}{8}\langle v(y)\rangle\frac{\alpha_0}{\ell} + \frac{b}{6\bar{t}}\right)\sum_s \exp\left(-\frac{s}{\delta}\right), \tag{9}$$

where the ratio $\alpha_0 = \langle v(y)^2\rangle/\langle v(y)\rangle^2$ is known as the "static tortuosity" [15–17] and for three-dimensional (3D) flow inside a straight tube α_0 has the exact value $4/3$. We assume that the value of α_0 for our macroscopically homogeneous porous medium remains of the order of $4/3$, and we incorporate this uncertainty into the factor a.

We can now solve the differential equation for $\langle\Theta(y,t)\rangle$ to obtain

$$\langle\Theta(y,t)\rangle = \exp\left[-t\left(\frac{a}{6}\frac{\langle v(y)\rangle}{\ell} + \frac{b}{6\bar{t}}\right)\sum_s \exp\left(-\frac{s}{\delta}\right)\right]. \tag{10}$$

We define the nondimensional time $\tau \equiv (t/\bar{t})\eta/6$ and the "disorder parameter" η

$$\eta \equiv a\frac{\langle v(y)\rangle}{v_\psi} + b, \tag{11}$$

where $v_\psi \equiv \ell/\bar{t}$. The factor $\eta/6$ thus represents the natural time scale of the process.

With the above definitions, we can rewrite (10) as

$$\langle\Theta(y,\tau)\rangle = \exp\left[-\tau\sum_s \exp\left(-\frac{s}{\delta}\right)\right]. \tag{12}$$

Taking the ensemble average of $\langle\Theta(y,\tau)\rangle$ (indicated by the operator $\{\ \}$) over all possible effective sites

$$\{\langle\Theta(y,\tau)\rangle\} = \left\{\exp\left[-\tau\sum_s \exp(-s_i/\delta)\right]\right\} \tag{13}$$

yields

$$\{\langle\Theta(y,\tau)\rangle\} = \int_V \frac{d^3s_1}{V}\cdots\int_V \frac{d^3s_N}{V}\exp\left[-\tau\sum_{i=1}^{N}\exp(-s_i/\delta)\right], \tag{14}$$

where the volume V is the total volume, i.e., $V = NV_{cell}$, with N being the number of effective sites. The definition of an effective site is one that is separated on average by $(3V_{cell}/4\pi)^{1/3}$ from a neighboring one.

Rewriting (14) as

$$\{\langle\Theta(y,\tau)\rangle\} = \int_V \frac{d^3s_1}{V}\cdots\int_V \frac{d^3s_N}{V}\prod_{i=1}^{N}\exp[-\tau\exp(-s_i/\delta)], \tag{15}$$

and adding and subtracting 1 on the right-hand side gives

$$\{\langle\Theta(y,\tau)\rangle\} = \prod_{i=1}^{N}\left[1 - \int_V \frac{d^3 s_i}{V}(1-\exp(-\tau\exp(-s_i/\delta)))\right]. \tag{16}$$

We then multiply and divide by N to get

$$\{\langle\Theta(y,\tau)\rangle\} = \prod_{i=1}^{N}\left[1 - \frac{N}{N}\frac{1}{V} \times \int_V d^3 s_i(1-\exp(-\tau\exp(-s_i/\delta)))\right]. \tag{17}$$

At this point we assume the ergodic hypothesis for which all the sites are equivalent to get

$$\{\langle\Theta(y,\tau)\rangle\} = \left[1 - \frac{N}{NV}\int_V d^3 s\left(1-\exp\left(-\tau\exp\left(-\frac{s}{\delta}\right)\right)\right)\right]^N. \tag{18}$$

Taking the limit to the number of sites $N\to\infty$,

$$\{\langle\Theta(y,\tau)\rangle\} = \exp\left[-\frac{N}{V}\int_V d^3 s\left(1-\exp\left(-\tau\exp\left(-\frac{s}{\delta}\right)\right)\right)\right]. \tag{19}$$

We consider an isotropic system and we make the change of variables $x=s/\delta$,

$$\{\langle\Theta(y,\tau)\rangle\} = \exp\left[-\frac{4\pi\delta^3 N}{V}\int_0^\infty \big(1-\exp(-\tau\exp(-x))\big)x^2 dx\right]. \tag{20}$$

Anticipating the outcome of the experimental results, we make the *ansatz* that the radius r of the sphere of volume $V_{cell}=(4/3)\pi r^3$ is proportional to the correlation length δ through the nondimensional rescaling time $\eta/6$ defined following (11), i.e., $r\equiv 6\delta/\eta$. As discussed earlier, the radius r is proportional to ℓ, justifying the introduction of the η parameter. It will be seen from the experiments that the fluid velocity $\langle v\rangle$ is of the order of the transport velocity v_ψ, i.e., $\eta\sim 1$. The averaging radius r therefore encompasses several correlation lengths δ.

We thus rewrite (20) as

$$\{\langle\Theta(y,\tau)\rangle\} = \exp\left[-\frac{4\pi r^3 N}{V}\left(\frac{\eta}{6}\right)^3 \times \int_0^\infty \big(1-\exp(-\tau\exp(-x))\big)x^2 dx\right]. \tag{21}$$

In the range $0.8<\eta<1.5$, we can use the approximation $(\eta/6)^3\approx 1/6(\eta+2.3)$ with a relative error of 2×10^{-3}. We also incorporate the constant 2.3 into the definition of b in (11). From the definition of r we have that $V=NV_{cell}=N4/3\pi r^3$, hence

$$\{\langle\Theta(y,\tau)\rangle\} = \exp\left[-\frac{\eta}{2}\int_0^\infty \big(1-\exp(-\tau\exp(-x))\big)x^2 dx\right]. \tag{22}$$

The integral in (22) can be expressed as [14]

$$\{\langle\Theta(y,\tau)\rangle\} = \exp\left[-\frac{\eta}{2}\frac{\tau}{3}\left(-\frac{d^3}{da^3}(\tau)^{-a}\gamma(a,\tau)\right)_{a=1}\right], \tag{23}$$

where γ is the incomplete Gamma function [18]. Equation (23) is equal to

$$\{\langle\Theta(y,\tau)\rangle\} = \exp\left[-\eta\tau\,{}_4F_4\left[\begin{matrix}1,1,1,1\\2,2,2,2\end{matrix};-\tau\right]\right], \tag{24}$$

where ${}_pF_q$ is the generalized hypergeometric function defined as

$${}_pF_q\left[\begin{matrix}a_1,a_2,\ldots,a_p\\b_1,b_2,\ldots,b_q\end{matrix};x\right] = \sum_0^\infty \frac{(a_1)_k(a_2)_k\ldots(a_p)_k}{(b_1)_k(b_2)_k\ldots(b_q)_k}\frac{x^k}{k!}, \tag{25}$$

and $(a)_k=\Gamma(a+k)/\Gamma(a)=a(a+1)\ldots(a+k-1)$ is the Pochhammer symbol, also known as the rising factorial.

The normalized transition probability $\psi(\tau)$ is defined by [14]

$$\frac{6\overline{t}}{\eta}\psi(\tau) \equiv -\frac{d\{\langle\Theta(y,\tau)\rangle\}}{d\tau}. \tag{26}$$

Developing the derivative in (26) we obtain

$$\frac{6\overline{t}}{\eta}\psi(\tau) = \eta\,{}_3F_3\left[\begin{matrix}1,1,1\\2,2,2\end{matrix};-\tau\right]e^{-\eta\tau}\,{}_4F_4\left[\begin{matrix}1,1,1,1\\2,2,2,2\end{matrix};-\tau\right]. \tag{27}$$

The hypergeometric functions ${}_3F_3$ and ${}_4F_4$ are always positive and tend for small times to the value 1, reducing $\psi(\tau)$ to a pure exponential. The limits of these functions for $\tau\to\infty$ are also constants equal to $\pi^2/12$ and $\zeta(3)/3$, for ${}_3F_3$ and ${}_4F_4$, respectively, with the ζ function defined as in Abramowitz and Stegun [18]. We recall that the spreading behavior is purely Fickian when the $\psi(\tau)$ is a pure exponential. Thus, Eq. (27) can actually account for the transition from a purely diffusive regime (at extremely small times when the tracer does not yet "see" the microscopic heterogeneities around the spreading source) to (eventually) another "homogenized" regime in which the length scales involved in the overall transport are much larger than the correlation length of the disordered porous system. The regime of most practical interest, however, lies in the broad transition between these two extremes in which anomalous transport prevails.

An illustration of the $\psi(\tau)$ behavior is given in Fig. 3 for several values of the η parameter. We note that $\psi(\tau)$ approaches an exponential behavior as η increases, whilst smaller values of η are associated with systems with higher degrees of disorder. In terms of (11), values of η of the order of unity correspond to a physical situation in which v_ψ is of the order of magnitude of the average pore velocity $\langle v\rangle$.

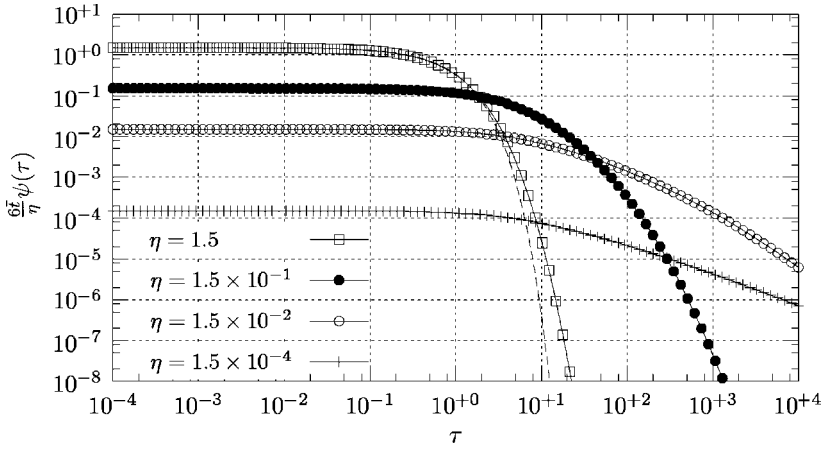

FIG. 3. Evolution of the dimensionless transition probability $(6\bar{t}/\eta)\psi(\tau)$ vs dimensionless time τ in (27) for different values of the η parameter. The dashed line represents the exponential limit of the function for $\eta=1.5$.

B. The generalized advection-dispersion equation with memory

It can be shown [13,19] that the ensemble average of the ME for the resident concentration can be written as a generalized ME that is equivalent to a CTRW. Dentz *et al.* [20] showed that the CTRW formalism can be described efficiently in terms of a partial differential equation with a memory term

$$n[\langle u\tilde{c}(y,u)\rangle - \langle c_0(y)\rangle] = -\tilde{M}(u)\,\nabla\cdot[q_\psi\langle\tilde{c}(y,u)\rangle - D_\psi\nabla\langle\tilde{c}(y,u)\rangle]. \tag{28}$$

The memory function $\tilde{M}(u)$ is

$$\tilde{M}(u) = \bar{t}u\frac{\tilde{\psi}(u)}{1-\tilde{\psi}(u)}, \tag{29}$$

where $\tilde{\psi}(u)$ is given by the Laplace transform of (27) (u is the Laplace parameter), and

$$q_\psi = \frac{1}{\bar{t}}\sum_s p(s)s = nv_\psi(y),\ D_\psi = \frac{1}{\bar{t}}\sum_s \frac{1}{2}p(s)ss \equiv \alpha_\psi q_\psi, \tag{30}$$

where the tensor

$$\alpha_\psi = \frac{\sum_s \frac{1}{2}p(s)ss}{|\sum_s p(s)s|}, \tag{31}$$

has dimension of length. The Laplace transform of the $\psi(\tau)$ in (27) is evaluated numerically for all values of u using an adaptive Clenshaw-Curtis quadrature scheme [21]. In the limit of $\psi(\tau)\to e^{-\tau}$, then $\tilde{M}(u)=$const and (28) is formally equivalent to the classical ADE in (1). This can be seen easily by substituting the Laplace transform of the pure exponential $\tilde{\psi}(u)=(1+u)^{-1}$ into (29) to obtain $\tilde{M}(u)=1$.

For a 1D system, given a constant flux-boundary condition at the inlet, i.e., $\tilde{j}\equiv\tilde{M}v(\tilde{c}-\alpha_\psi\partial\tilde{c}/\partial y)=u^{-1}$, at $y=0$, a natural boundary condition at the outlet, i.e., $\partial\tilde{c}/\partial y=0$ at $y=L\equiv 1$, and an initial condition $c_0(y)=0$, Eq. (28) admits the exact analytical solution

$$\tilde{j}(u) = \frac{1}{u}\frac{2z\exp\left(\frac{1}{2}(\alpha_\psi^{-1}+z)\right)}{[\exp(z)(z+\alpha_\psi^{-1}+2u/(\tilde{M}v_\psi)) + (z-\alpha_\psi^{-1}-2u/(\tilde{M}v_\psi))]}, \tag{32}$$

where

$$z = \frac{1}{\alpha_\psi}\sqrt{1+\frac{4u\alpha_\psi}{\tilde{M}v_\psi}}. \tag{33}$$

Equation (32) is then numerically inverted to the time domain by means of an inverse Laplace transform algorithm [22,23]. A series of plots for different values of the nondimensional parameter η are given in Fig. 4, for nondimensional velocity and dispersivity equal to $v_\psi/L=1$, and $\alpha_\psi/L=0.05$, respectively.

IV. DISCUSSION

We now analyze the 48 short column experimental BTCs. Fitting numerical solutions of (32) to these experimental BTCs, we obtained independently the parameters v_ψ, D_ψ, and η corresponding to the $\psi(\tau)$ in (27), and the parameters $\langle v\rangle$ and D for the ADE in (1) (i.e., the solution of (32) for $\tilde{M}(u)=1$). Note that, as mentioned in the Introduction, Eq. (32) is exact for the boundary conditions and system geometry of these experiments.

In Fig. 1, we show a typical example of the fit obtained by means of (28). It can be seen that the solution of (28) with a memory function defined by the $\psi(\tau)$ in (27) captures all of the "anomalous" features (in contrast to the ADE model) and also better describes the position of the mean arrival.

In Fig. 5 we plot the value of the disorder parameter η against the ratio $\langle v\rangle/v_\psi$ for the set of 48 BTCs: it can be seen that the prediction of (11) is clearly satisfied by our experiments. The fitted values of η range between 0.8 and 1.5. This range of values is characteristic of a weak disorder. The regression line plotted in Fig. 5 has a slope $a=1.0071$ and an intercept $b=0.1069$. We note that the value of η does not show any specific dependence on the values of mean grain

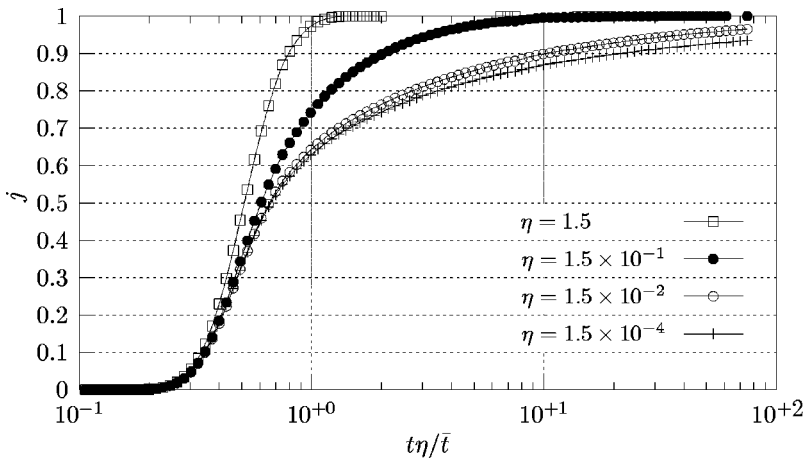

FIG. 4. Breakthrough curves solutions of (32), where the quantity j represents the normalized flux-averaged concentration, using the transition-probability function $\psi(\tau)$ in (27), vs nondimensional time $\tau = t\eta/\bar{t}$ for different values of the disorder parameter η, with $v_\psi/L = 1$ and $\alpha_\psi/L = 0.05$.

size d_m, porosity n, tortuosity α_∞, characteristic viscous length Λ, or permeability k_0 (as defined in the Appendix). These factors only enter implicitly into the determination of a and b. The fact that $a \approx 1$ is consistent with our choice of constants in (3). These findings show that the parameter a is not scale dependent and should therefore depend in a universal way on a combination of the aforementioned parameters, for instance, $a \approx 8k_0/(n\Lambda^2\alpha_\infty)$, which for smooth porous media is typically in the order of unity [24]. The coefficient b carries the information on the diffusion contribution to the transition rates, so we expect to find different numerical values for different choices of the solute pure-diffusion coefficient.

The surprising robustness of the expression in (11) indicates that the main dependence of the η parameter is effectively on the ratio of fluid velocity to transport velocity, $\langle v \rangle / v_\psi$. The approximations made in the determination of η are consistent with values needed to fit the data in a system with small disorder. The importance of our results lies in demonstrating that mild fluctuations from a completely "homogeneous" porous medium have clear effects on the basic observations of transport in these media. This study indicates that the physical picture that is the basis of the classical ADE leads to an incomplete description of transport phenomena even in "homogeneous" media, whereas the proposed CTRW description can describe this kind of transport.

ACKNOWLEDGMENTS

The authors thank the European Commission—Marie Curie Programme (A.C.) and the Israel Science Foundation (Grant No. 147/01) (B.B.).

APPENDIX

In the definition of the $w(y+s)$ the main dependence is on the fluid velocity $v(y+s)$. However, this "forcing term" must be rescaled with a characteristic length of the spatial transitions; this length depends on the assumed idealization of the porous medium. For example, for a medium consisting of a network of pores and straight tubes, the length ℓ is a characteristic distance of the interpore distance, i.e., the length of the tubes. Because the rescaling is governed by ℓ, the dependence of the constant a is only on "averaged" quantities such as the permeability k_0, the porosity n, the characteristic viscous length Λ, and the tortuosity α_∞. For smooth porous media the ratio $8k_0/(\alpha_\infty n\Lambda^2) \approx 1$ [see, e.g., 24].

The permeability is defined as $k_0 = n\langle v_0 \rangle L_y^2$ and is computed by solving the Stokes problem $\eta\nabla^2 v_0 - \nabla p + e = 0$, and $\nabla \cdot v_0 = 0$, the quantity e being a unit force vector. No-slip boundary conditions at the pore walls, and periodicity of v_0 and p, are prescribed. It is logical to introduce the permeability in the denominator as the higher the medium permeabil-

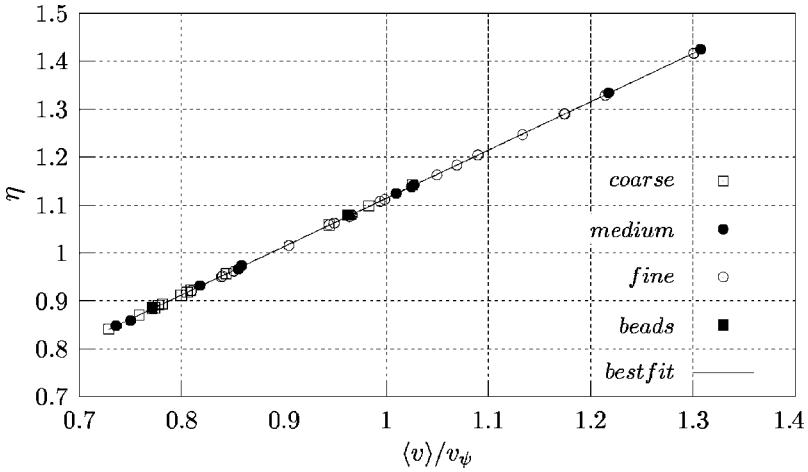

FIG. 5. Coefficient η vs the dimensionless velocity $\langle v \rangle / v_\psi$ for a set of 48 experimental breakthrough curves on short columns filled with well-sorted granular materials of different grain size. The slope of the curve sets the value for parameter a. The linear regression analysis yields $a = 1.0071$ and an intercept value equal to $b = 0.1069$.

ity, the higher the probability of a particle transition.

The characteristic viscous length is defined as $2/\Lambda = \int |v_\infty|^2 dS / \int |v_\infty|^2 dV$, where the latter integral describes a velocity-weighted surface(S)-to-volume(V) ratio. The velocity field $v_\infty = \nabla \psi$ follows from the potential problem $\nabla^2 \psi = 0$, with Neumann boundary conditions on the fluid-solid interface and periodicity on the inlet-outlet surfaces of the averaging cell. The characteristic viscous length is the "natural" length scale for the permeability.

The tortuosity is defined as $\alpha_\infty = \langle |v_\infty|^2 \rangle / |\langle v_\infty \rangle|^2 > 1$. We require the tortuosity to account for the fact that particle transitions do not occur over straight lines along the principal direction of flow.

For porous media whose pore-fluid surfaces present sharp singularities due, for instance, to the presence of clays, the ratio $8k_0/(\alpha_\infty n \Lambda^2)$ deviates significantly from the value 1 [25,26]. We argue that, for these particular geometries, the slope a of the regression line might deviate accordingly.

[1] G. I. Taylor, Proc. R. Soc. London **A219**, 186 (1953).

[2] A. E. Scheidegger, *Proceedings of the Theory of Fluid Flow in Porous Media Conference* (Univ. Oklahoma, Oklahoma, 1959), pp. 101.

[3] F. Hoffman, D. Ronen, and Z. Pearl, J. Contam. Hydrol. **22**, 95 (1996).

[4] S. Oswald, W. Kinzelbach, and G. Brix, Geoderma **80**, 417 (1997).

[5] S. E. Silliman and E. S. Simpson, Water Resour. Res. **23**, 1667 (1987).

[6] M. Levy and B. Berkowitz, J. Contam. Hydrol. **64**, 203 (2003).

[7] A. Cortis and B. Berkowitz, Soil Sci. Soc. Am. J. **68**, 1539 (2004).

[8] D. R. Nielsen and J. W. Biggar, Soil Sci. Soc. Am. Proc. **25**, 1 (1961).

[9] P. M. Jardine, G. K. Jacobs, and G. V. Wilson, Soil Sci. Soc. Am. J. **57**, 945 (1993).

[10] B. Berkowitz and H. Scher, Phys. Rev. Lett. **79**, 4038 (1997).

[11] B. Berkowitz, H. Scher, and S. E. Silliman, Water Resour. Res. **36**, 149 (2000).

[12] G. Kosakowski, B. Berkowitz, and H. Scher, J. Contam. Hydrol. **47**, 29 (2001).

[13] B. Berkowitz, J. Klafter, R. Metzler, and H. Scher, Water Resour. Res. **38**, 1191 (2002).

[14] H. Scher and M. Lax, Phys. Rev. B **7**, 4502 (1973).

[15] A. Norris, J. Wave-Mater. Interact. **1**(4), 365 (1986).

[16] D. Lafarge, Ph.D. thesis, Université du Maine, Le Mans, France, 1993 (unpublished).

[17] A. Cortis, *Dynamic Acoustic Parameters of Porous Media: A Theoretical, Numerical, and Experimental Investigation* (Delft University Press, Delft, 2002).

[18] M. Abramowitz and I. Stegun, *Handbook of Mathematical Functions* (Dover, New York, 1970).

[19] J. Klafter and R. Silbey, Phys. Rev. Lett. **44**, 55 (1980).

[20] M. Dentz, A. Cortis, H. Scher, and B. Berkowitz, Adv. Water Resour. **27**, 155 (2004).

[21] W. H. Press, S. A. Teukolsky, W. T. Vetterling, and B. P. Flanner, *Numerical Recipes in C: The Art of Scientific Computing* (Cambridge University Press, Cambridge, 2002), 2nd ed.

[22] F. R. de Hoog, J. H. Knight, and A. N. Stokes, SIAM (Soc. Ind. Appl. Math.) J. Sci. Stat. Comput. **3**, 357 (1982).

[23] A. Cortis, C. Gallo, H. Scher, and B. Berkowitz, Water Resour. Res. **40**, W04209 (2004).

[24] D. Johnson, J. Koplik, and R. Dashen, J. Fluid Mech. **176**, 379 (1987).

[25] A. Cortis and D. Smeulders, Int. J. Eng. Sci. **39**, 951 (2001).

[26] A. Cortis, D. Smeulders, J.-L. Guermond, and D. Lafarge, Phys. Fluids **15**, 1766 (2003).